Microstripline-Coupled Quasi-Optical Niobium Hot Electron Bolometer Mixers around 2.5 THz

W.F.M. Ganzevles[†], J.R. Gao[§], P. Yagoubov[§], T.M. Klapwijk[†] and P.A.J. de Korte[§]

Department of Applied Physics and Delft Institute for Microelectronics and Submicron Technology (DIMES),
[†]Delft University of Technology,
Lorentzweg 1, 2628 CJ Delft, The Netherlands
[§]Space Research Organization of the Netherlands,
Postbus 800, 9700 AV Groningen, The Netherlands

Abstract

For the first time, the measured direct and heterodyne response of a hot electron bolometer mixer (HEBM) at 2.5 THz applying a microstripline coupling circuit is reported. A new fabrication process for quasi-optically coupled HEBMs essentially consisting of a twin slot antenna, microstripline transformer and Nb microbridge has been developed. In a Fourier transform spectrometer, the frequency response of the device is measured. We find a peak response at a frequency of 2.0 THz and the bandwidth equals 1.5 THz. The peak frequency is about 20% lower than predicted by a model based on coupling the impedance of the constituting elements. By applying 2.5 THz RF radiation from a FIR laser, the mixer can be fully pumped as is suggested by the current-voltage curves. Using a chopped Y-factor technique, an uncorrected noise temperature $T_{N,rec}$ of 4200 K has been measured.

1   INTRODUCTION

Superconducting HEBMs are very promising candidates to fulfill the need for low-noise, high frequency detectors in astronomical missions like FIRST.

Practical application of these devices requires a suitable antenna like a twin-slot antenna. To match the antenna-impedance to the bridge impedance, a transmission line is needed. In the literature, the use of Co-Planar Waveguide (CPW) transmission lines at 2.5 THz is reported (Ref. 1, 2). An alternative is the use of microstripline transmission lines. So far, this coupling structure has only been used in SIS mixers and has never been introduced in HEBMs.

There are various reasons to change from CPW-transmission lines to microstriplines in high-frequency receivers. First, in a CPW-design, there is a disturbance of the antenna properties due to the fact that all other structures also are situated in the ground plane. This might have an impact on the antenna beam

pattern. This disadvantage does not take place in a design based on the microstrip-line. Second, it allows for a much larger variation in characteristic impedance of the transmission line, making it easier to match a diffusion cooled HEB, which usually has a low impedance. Besides, filter characteristics and matching can be improved significantly due to the large impedance ratios achievable. Third, the microstrip transmission line has proven to work very well in an SIS-mixer up to about 1 THz (Refs. 3, 4). Then, with respect to the fabrication, the microstripline design could be easier than that of the CPW transmission line because the structures can be defined by conventional optical lithography without the need of a high-resolution lithography such as e-beam lithography as is required for CPW-based devices. Lastly, microstriplines are widely used and the simulation models are well developed, where CPW calculations have proven to be difficult for structures having very small slots.

First, we will sketch the sample production, followed by the dc characteristics of the device. Then, we describe the simulation procedure used to predict the direct response and the measured response obtained in an Fourier transform spectrometer. We report the characteristics of the device using it as a mixer. Finally, we discuss and conclude the results obtained.

2 MICROSTRIPLINE-COUPLED HEBM LAY-OUT AND FABRICATION

The lay-out of the coupling structure (Fig. 1) is described as follows. A twin slot antenna is used to receive the signal. For symmetry reasons, this design intrinsically implies that no direct antenna-bridge contact can be made. To guide the signal from the antenna to the microbridge, we have made a new design in HEBM technology. A microstrip line transformer is introduced to match the antenna impedance to the microbridge impedance. The microstrip line consists of an Au ground plane, in which the antenna is defined, an Al/Nb top wiring, and a SiO_2 dielectric separating the top wiring from the ground plane. A microstrip line RF filter avoids leakage of the RF signal into this IF chain.

A fabrication process for Nb HEBMs has been developed using two-step electron beam lithography (EBL) to define both bridge length and width. Near UV lithography is used to define the rest of the device.

We use a high-resistivity, double-sided polished Si substrate. In the first step, a ground plane of 250 nm thick Au is evaporated on a layer of 5 nm sputtered Al, which serves as an adhesion layer. The ground plane contains the twin slot antenna and the IF CPW as well as alignment markers for consequent steps. In order for the SiO_2 dielectric to stick, 1.5 nm Ti is evaporated and subsequently oxidized, so that no RF currents will run in the lossy Ti (Ref. 5). In a lift-off process, a dielectric of 250 nm SiO_2 is sputtered on the areas where the microstripline will be located. Then we deposit 16 nm Nb using dc sputtering. Using a lift-off mask, patches of 12 μm $\times$12 μm on top of the SiO_2 are covered. Au cooling pads are then
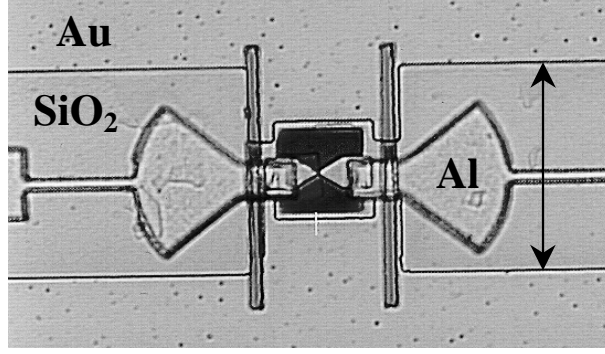
Figure 1: *Optical micrograph of a microstripline-coupled HEBM. The arrow represents 31 µm. Left and right of the dark (Nb) square, the antenna slots in the ground plane are visible. On top of the big* SiO$_2$ *rectangles, the Al/Nb top wiring is visible. Radial stubs serve as rf shorts to the ground plane, picking up radiation from the antenna. They also form the first section of the rf filter. The triangles form the cooling pads, defining the bridge length. Since this picture has been taken before defining the width of the microbridge, the Nb square is still visible.*

defined using EBL in a double layer PMMA system. RF cleaning of the Nb in an Ar-plasma is performed to remove the native Nb oxide, in order to achieve a high interface transparency. In situ, ~ 10 nm Au is sputtered. Then, in a separated system, 80 nm Au is e-beam evaporated at a pressure of 2×10^{-6} mbar.

The top wiring layer of the microstripline is a layer of 550 nm Al, on top of which 75 nm Nb is sputtered to reduce DC- and IF series resistance. This top wiring is defined in an optical lift-off process. The deposition of this layer is the bottleneck of our process. In contrast to the typical SIS process, the superconducting bridge is in series with the top wiring. This means that contact between top- and bottom layer is established via a step coverage on the vertical wall of the SiO$_2$, which turns out to be rather difficult. As a last optical step, we deposit 90 nm Nb on the IF CPW-transmission line, again to avoid loss at IF. In the last production step, we define the bridge width. Using EBL, we define a PMMA bridge in the double layer resist system as before. Only the Nb parts that have to be etched are opened up. In a mixture of CF$_4$+3%O$_2$, the Nb is reactive ion etched. We monitor the process by measuring the optical reflectivity of the Nb on the SiO$_2$ by using a laser interferometer as an endpoint detection system. Using this process we are able to produce Nb bridges as small as 60 nm$\times$ 80 nm (Ref. 6).

After wire bonding, dc measurements are performed in a metal vacuum box. dc measurements are used as a quality assessment of the devices. A typical unpumped IV-curve, taken at 3 K, is shown in Fig. 3. The normal resistance is about 15 Ω , the critical current about 70 μA and the critical temperature T$_c$ = 4.6 K. These values are similar to the ones measured in the CPW-coupled devices we measured (Ref. 2).

The RT- and IV curves found in this batch show some degradation compared to previous batches. We speculate this is related to interference of multiple processes executed in our sputtering chamber.

3 DIRECT RESPONSE

The geometry we use has been designed using a method that splits the structure in four separate parts. First, the microbridge itself is considered. We assume its impedance can be expressed as $Z_{\text{HEB}} = R_N$ (Ref. 2) where Z_S is the surface impedance of the superconducting bridge and R_N equals the normal state resistance.

Second, the impedance of the antenna as a function of frequency is calculated using a moment method in the Fourier transform domain, developed by Kominami et al. (Ref. 7). For details, see Refs. 2 and 8. Throughout this paper, it is assumed that the peak response of the antenna is in practice 12% lower than predicted (Refs. 2, 8).

Third, the impedance of the microstripline is calculated based on models generally used for microstripline calculation (see e.g. Refs. 9 and 10). The characteristic impedance of the line is calculated as a function of frequency, line width and thickness of metal and dielectric layers including an effective $\varepsilon_{r,\text{SiO}_2}$ and fringing field effects. By varying these parameters, the impedance can be tuned from about $5\,\Omega$ to $35\,\Omega$ without introducing orthogonal modes, i.e. without making the line wider than about $\lambda/4$. The ratio of obtainable characteristic impedance values in the microstripline is much larger than that reported for CPW lines, offering more freedom in transformer- and filter design.

Since we did not measure dc properties of the films used in the HEBMs, we use a dc conductivity $\sigma = 1 \times 10^8 \Omega^{-1} m^{-1}$ for both top and bottom wiring layer. These values have been measured for Al previously in our group (Refs. 11 and 12). From this, the surface impedance of the top- and bottom plane are calculated in the extreme anomalous according to:

$$Z_S = 1.5 \cdot \frac{1}{3^{\frac{1}{2}} \pi^{\frac{1}{3}}} \left(1 + \sqrt{3}i\right) \left(\frac{9\omega^2 \mu_0^2 l_e}{16\sigma}\right)^{\frac{1}{3}}, \tag{1}$$

in which ω, μ_0, l_e and σ are frequency, magnetic permittivity, electron mean free path (assumed to be $l_e = 125\,\text{nm}$) and dc conductivity, respectively. The additional factor 1.5 in Eq. 1 is an empirical multiplication factor added because the film is strictly speaking not in the extreme anomalous limit.

The RF filter we use is designed such that it reflects the RF signal back to the microbridge. This avoids signal being lost into the IF chain. It is important to note that the filter has low impedance. If not, the impedance match would be strongly influenced, since an infinite metal ground plane is assumed around the

slots, acting as a short. The filters are designed to have a small number of $\lambda/4$-sections to keep the series resistance due to the Al top wiring as low as possible. Although a low number of filter sections decreases the steepness at the cutoff frequencies, the impedance around the center frequency f_{center} is not affected. The filter is made of microstrip transmission line. The impedance of the separate sections is calculated using microstripline formulae (Ref. 9). The impedance of a microstripline filter with characteristic impedance Z_0, length l and terminated with a load Z_{load}, then, is given by repeated application of

$$Z_{\mathrm{filter}} = Z_0 \frac{Z_{\mathrm{load}} + \imath Z_0 \tan{(\gamma \cdot l)}}{Z_0 + \imath Z_{\mathrm{load}} \tan{(\gamma \cdot l)}} \tag{2}$$

where γ is the propagation constant.

The last part of the geometry consists of the microstripline transformer, which transforms the added antenna- and filter impedance into the impedance Z_{embed} seen by the bridge according to an equation similar to Eq. 2 with Z_{embed} instead of Z_{filter}, the characteristic impedance of the transformer instead of Z_0 and for Z_{load} we take $Z_{\mathrm{ant}} + Z_{\mathrm{filter}}$. In the calculations, the tapered structure of the cooling pads is approximated by a series of rectangles.

The intrinsic response η_{int} of the microstripline coupled HEBM can be calculated using

$$\eta_{\mathrm{int}} = 1 - \left| \frac{Z_{\mathrm{HEB}} - Z_{\mathrm{embed}}}{Z_{\mathrm{HEB}} + Z_{\mathrm{embed}}} \right|^2. \tag{3}$$

The direct response in current $\Delta I(f)$ of an HEBM measured in an FTS can be described by (Refs. 2,8)

$$\Delta I(f) \propto \eta_{\mathrm{int}} \cdot \eta_{\mathrm{opt}} \cdot \eta_{\mathrm{FTS}}, \tag{4}$$

with η_{opt} the combined transmission of the window and heat filter and η_{FTS} the power transfer function of the FTS.

Fig. 2 shows the response $\Delta I(f)$ of the device measured in an FTS at a bath temperature $T_{\mathrm{bath}} = 3\,\mathrm{K}$ and the direct response predicted by the model above. The setup is described elsewhere (Ref. 8).

The measured 3 dB-bandwidth B_{m} equals 1.6 THz and $f_{\mathrm{center,m}}$ is found to be 1.9 THz. The plot also shows the predicted response $\eta_{\mathrm{int,sim}} \cdot \eta_{\mathrm{opt}} \cdot \eta_{\mathrm{FTS}}$ with $B_{\mathrm{sim}} = 1.4\,\mathrm{THz}$ and $f_{\mathrm{center,sim}} = 1.95\,\mathrm{THz}$. The peak frequencies of both curves are comparable, assuming the dip not to be due to the HEB (Ref. 13). B_{m} is slightly larger than B_{sim}. Similar data has been obtained from several devices. If we assume the downshift in peak response is at least partly caused by the antenna, as is the case in the CPW coupling scheme (as mentioned, this is done throughout this paper) (Ref. 2), the data are well described by the model.

An even better agreement between measurement and model is obtained if we assume a reduction in the dc conductivity by a factor of 3 to 5. Intuitively, this
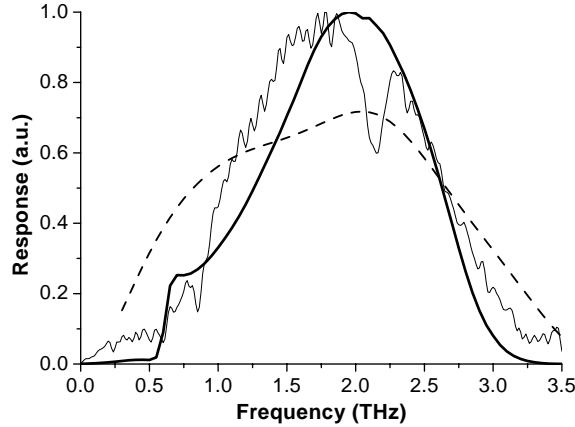
Figure 2: *Direct response as a function of frequency of a typical microstripline coupled HEB together with the transmission of the Fourier transform spectrometer and optics. Shown are the normalized measured data (solid thin), transmission of the optics and FTS $\eta_{\mathrm{opt}} \cdot \eta_{\mathrm{FTS}}$ (dashed thin) and normalized intrinsic response $\eta_{\mathrm{int,sim}}$ (solid thick).*

can be explained as follows: most of the RF current will run in the bottom layer of the top wiring. This part of the film will have a lower-than-average quality due to the sputter process and surface roughness of the SiO_2. Therefore, it does not see the average value of the dc-conductivity σ as measured in a dc experiment. The transmission line will then have a higher loss than expected based on the dc value of σ.

We suggest that the thickness of the metal layer has to be taken into account in the model, since the thickness becomes of the order of the antenna slot width, possibly changing the effective ε_r in the antenna slots (see Ref. 2).

The model for describing the microstrip line behavior around 2.5 THz seems to work reasonably well. However, because of the uncertainty in σ we cannot draw quantitative conclusions.

As expected, the influence of the metal conductivity is seen in the simulations in both center frequency and bandwidth.

We have also measured several devices with a slightly different design regarding the top wiring layer. Devices having a rectangular coupler instead of a radial stub (Fig. 1) do not show significant deviations from the observed direct response. A device having a filter with 6 $\lambda/4$ sections (instead of 2 sections as in the data shown) on either side shows a larger bandwidth (1.9 THz) and a lower f_{center} (1.5 THz).
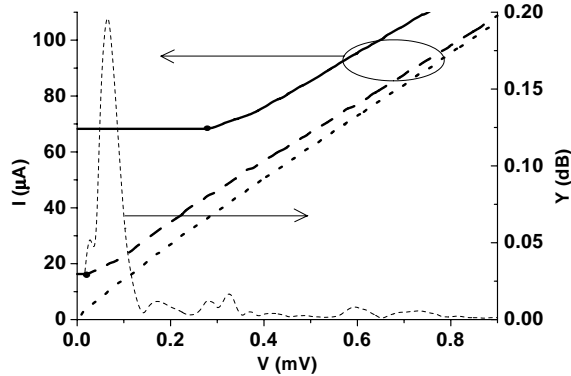
Figure 3: *IV-curves of the HEBM pumped with 2.5THz-radiation: unpumped (solid) IV curve, optimally pumped (dashed) and overpumped (dotted) measured at 3 K, IF=1.25 GHz. The thin dashed line shows the chopped Y-factor in the optimally pumped situation.*

4 HETERODYNE MEASUREMENTS

Heterodyne measurements are performed at 2.5 THz using a FIR laser. Using this laser it is possible to pump the IV curves of the devices fully flat using a 6 μm Mylar beam splitter. The laser stability is on the order of 0.1%/min, measured using a pyro-detector. To average out possible instabilities in the system, we use a chopped hot/cold load at 300K/77K. At the IF, both the ac- and dc part of the power are recorded. From the Y-factor, $Y = \frac{(P_{dc} + \alpha \cdot P_{ac})}{(P_{dc} - \alpha \cdot P_{ac})}$, the noise temperature is determined. For the noise measurements reported here we use α=1, although this α in practice is larger than 1. The IF-chain (Ref. 14) consists of a standard bias Tee, isolator and HEMT amplifier and has 79 dB gain and a noise temperature of 7 K.

Fig. 3 shows the unpumped, optimally pumped and overpumped current-voltage curves of the mixer. The thin dashed line represents the Y-factor as a function of bias voltage. An optimal, chopped Y-factor of 0.20 dB has been measured. This corresponds to an uncorrected Callen and Welton-noise temperature $T_{N,uncorr}$ of 4200 $\pm$ 1000 K. A receiver gain of -23 dB has been measured. This is a few times the best noise temperature measured using CPW transmission lines (Ref. 15).

An optimization of the antenna size may improve the coupling efficiency by as much as 2 dB, decreasing the noise temperature considerably. Increasing the critical temperature T_c allows us to measure in the regime where $T_c - T_{bath}$ is larger. This may lead to a lower T_N (Ref. 16).

5 DISCUSSION

Initially, it was believed that the fabrication of microstripline coupled samples would be easier than the CPW coupled devices since –except for the microbridge– no sub-micron structures are needed. However, the step coverage of the top wiring to the ground plane turns out to be difficult, even if the top metal is sputtered and of the same thickness as the dielectric. We believe that high ridges of SiO_2 remain at the edges of the areas where the SiO_2 layer is deposited. These are due to incomplete lift off and have been observed using an atomic force microscope. These ridges inhibit good contact to the ground plane. In the end, increasing the metal layer thickness to about twice the dielectric layer thickness and carefully brushing the wafer during SiO_2 lift off yields good step coverage.

The direct response of the microstripline coupled HEBM can be described well assuming a down shift in peak response of 10-12%. We believe that this can be solved by reducing the antenna size.

6 CONCLUSIONS

We have designed and produced a novel type of HEBM using microstripline coupling structures. The direct response of the device is well understood and can be described based on the current model if a downshift of about 12% is assumed. A heterodyne experiment using a FIR laser as an local oscillator shows a noise temperature of 4200 K.

7 ACKNOWLEDGMENTS

REFERENCES

[1] B.S. Karasik, M.C. Gaidis, W.R. McGrath, B. Bumble, and H.G. LeDuc. IEEE Trans. on Appl. Supercond., **7**:3580, 1997.

[2] W.F.M. Ganzevles, L.R. Swart, J.R. Gao, T.M. Klapwijk, and P.A.J. de Korte. To appear in Appl. Phys. Lett., May 2000.

[3] J. Zmuidzinas and H.G. LeDuc. IEEE Trans. on Microwave Theory Tech., **40**:1797, 1992.

[4] M. Bin, M.C. Gaidis, J. Zmuidzinas, T.G. Phillips, and H.G. LeDuc. Appl. Phys. Lett., **68**:1714, 1996.

[5] P. Echternach, Private communication.

[6] W.F.M. Ganzevles, J.R. Gao, D. Wilms Floet, G. de Lange, A.K. van Langen, L.R. Swart, T.M. Klapwijk, and P.A.J. de Korte. Proceedings of the 10th International Symposium on Space Terahertz Technology, Charlottesville, VA, March 16-18, 1999, pages 247–260, 1999.

[7] M. Kominami, D.M. Pozar, and D.H. Schaubert. IEEE Transactions on Antennas and Propagat., **33**:600, 1985. We used a computer code of this method supplied by Zmuidzinas and Chattopadhyay.

[8] To appear in: Proceedings of the 11th International Symposium on Space Terahertz Technology, Ann Arbor, MI, May 2000, 2000.

[9] D.M. Pozar. *Microwave Engineering*. Addison-Wesley, 1990.

[10] G. Yassin and S. Withington. Electromagnetic models for superconducting millimetre-wave and submillimeter wave microstrip transmission lines. *ESA Technical Report RDG 4*, 1995.

[11] P. Dieleman. *Fundamental Limitations of THz Niobium and Niobiumnitride SIS Mixers*. PhD thesis, University of Groningen, 1998.

[12] B.D Jackson. Private communication.

[13] We do not attribute the dip to the device since devices with very different parameters and even different transmission lines show the dip at the same frequency.

[14] The IF chain consists of an isolator, Berkshire cryo-amplifier (44dB), Radiall bias Tee, room temperature amplifier (44dB), band pass filter (80 MHz at 1.25 GHz) and a Hewlett Packard power meter.

[15] R.A. Wyss, B.S. Karasik, W.R. McGrath, B. Bumble, and H. LeDuc. Proceedings of the 10th International Symposium on Space Terahertz Technology, Charlottesville, VA, March 16-18, 1999, pages 215–228, 1999.

[16] D. Wilms Floet, J.R. Gao, W.F.M. Ganzevles, T.M. Klapwijk, G. de Lange, and P.A.J. de Korte. Proceedings of the 10th International Symposium on Space Terahertz Technology, Charlottesville, VA, March 16-18, 1999, page 228, 1999.